Elsevier Editorial System(tm) for Applied Clay Science

Manuscript Draft

Manuscript Number: CLAY14123R1

Title: Photo-Oxidative Degradation of Injection Molded Sepiolite/Polyamide66 Nanocomposites

Article Type: VSI:Euroclay2019

Section/Category:

Keywords: Polyamide66, Sepiolite, Clay/Polymer Nanocomposites, UV exposure, Photo-oxidation

Corresponding Author: Professor M.Dolores La Rubia, Ph.D.

Corresponding Author's Institution: University of Jaén

First Author: Cristina Fernandez-Barranco, Ph.D

Order of Authors: Cristina Fernandez-Barranco, Ph.D; Africa Yebra-Rodriguez, Ph.D; Juan Jimenez-Millan, Ph.D; Francisco Javier Navas-Martos, Ph.D; Ana Yebra, Ph.D; Anne Koziol, Ph.D; M.Dolores La Rubia, Ph.D.

Manuscript Region of Origin: SPAIN

Abstract: Every day clay/polymer nanocomposites are included in more industrial applications, due to its high performance. Because of this, nanocomposites may be submitted to extreme conditions of work, which could degrade it. Exposure to solar radiation in the presence of oxygen (photo-degradation) represents one of the major problems of the Clay/Polymer anocomposites. In this study, samples of neat polyamide 66 (PA66-S-0) and reinforced nanocomposites with 1, 3, 5, 7 and 9 wt.% organophilized sepiolite (PA66-S-1, PA66-S-3, PA66-S-5, PA66-S-7 and PA66-S-9 samples) are analysed after UV exposure, following the standard accelerated degradation method UNE-EN-ISO 4892-2. The aim of this study is to establish the effect of UV exposure on the mechanical, optical and crystallographic properties of the new material. Tensile tests show a reduction in the ductility and an embrittlement after degradation process. In addition, an increase of transparency is confirmed with the UV exposure. The carbonyl index in the samples containing sepiolite is lower than in neat PA66 whereas the yellowness index is not affected by degradation. Sepiolite has an inhibitor effect on the formation of C=O bonds. These results indicate that breaking of chains of PA66 starts in the amorphous region and that it is lower in the nanocomposites due to the low diffusion of oxygen induced by the sepiolite. This affirmation is corroborated by the obtained diffraction patterns.

Photo-Oxidative Degradation of Injection Molded Sepiolite/Polyamide66 Nanocomposites

C. Fernández-Barranco[a], A. Yebra-Rodríguez[a], J. Jiménez-Millán[a], F. J. Navas-Martos[b], A. Yebra[c], A. E. Koziol[d], M. D. La Rubia[*e]

[a] Department of Geology and CEACTEMA, Faculty of Experimental Sciences, University of Jaen, Campus Las Lagunillas s/n, 23071 Jaen, Spain; cfernand@ujaen.es, ayebra@ujaen.es, jmillan@ujaen.es

[b] Centro Tecnológico del Plástico Andaltec, Avda. Principal s/n, Ampliación Polígono Cañada de la Fuente, 23600 Martos Jaén, Spain; francisco-javier.navas@andaltec.org

[c] Department of Optics, Faculty of Sciences, University of Granada, Campus Fuentenueva s/n, 18071 Granada, Spain; ayebra@ugr.es

[d] Departament of Crystallography, Maria Curie-Sklodowska University, Maria Curie Sklodowska Square 3, Lublin 20-031, Poland; anna.koziol@poczta.umcs.lublin.pl

[e] Department of Chemical, Environmental and Materials Engineering, Higher Polytechnic School of Jaen, University of Jaen, Campus Las Lagunillas s/n, 23071 Jaen, Spain; mdrubia@ujaen.es

Abstract

Every day clay/polymer nanocomposites are included in more industrial applications, due to its high performance. Because of this, nanocomposites may be submitted to extreme conditions of work, which could degrade it. Exposure to solar radiation in the presence of oxygen (photo-degradation) represents one of the major

problems of the Clay/Polymer anocomposites. In this study, samples of neat polyamide 66 (PA66-S-0) and reinforced nanocomposites with 1, 3, 5, 7 and 9 wt.% organophilized sepiolite (PA66-S-1, PA66-S-3, PA66-S-5, PA66-S-7 and PA66-S-9 samples) are analysed after UV exposure, following the standard accelerated degradation method UNE-EN-ISO 4892-2. The aim of this study is to establish the effect of UV exposure on the mechanical, optical and crystallographic properties of the new material. Tensile tests show a reduction in the ductility and an embrittlement after degradation process. In addition, an increase of transparency is confirmed with the UV exposure. The carbonyl index in the samples containing sepiolite is lower than in neat PA66 whereas the yellowness index is not affected by degradation. Sepiolite has an inhibitor effect on the formation of C=O bonds. These results indicate that breaking of chains of PA66 starts in the amorphous region and that it is lower in the nanocomposites due to the low diffusion of oxygen induced by the sepiolite. This affirmation is corroborated by the obtained diffraction patterns.

Keywords

Polyamide66, Sepiolite, Clay/Polymer Nanocomposites, UV exposure, Photo-oxidation.

1. Introduction

The number of applications that require advanced materials capable of withstanding the work conditions to which they are subjected is increasing daily. Much research in materials science and engineering therefore focuses on finding new advanced materials (Okada and Usuki, 2006; Kotal and Bhowmick, 2015; Valino et al., 2019). Improving the mechanical properties of clay/polymer nanocomposites (CPN) makes them ideal for many applications (Butnaru et al., 2016; Fernández-Barranco et al,

2014; Mukhopadhyay et al., 2020; Pfaendner, 2010; Sharma et al., 2019), and they are now expanding to numerous outdoor applications. Their usefulness depends, however, on their durability in a particular environment, or their interaction with environmental factors. The versatility of these advanced materials makes it possible that they will be exposed to UV radiation which, in the presence of atmospheric oxygen, causes them to degrade, affecting their properties through photo-oxidative degradation, one of the primary sources of damage to polymers in outdoor applications (Bocchini et al., 2010; Bussière et al, 2013; Olewnik-Kruszkowska, 2015; Pandey et al, 2005; Remili et al., 2009; Zaidi et al., 2010). Studying the degradation and stability of these materials is thus an issue of great interest from the scientific and industrial point of view, since better knowledge of the degradation mechanisms will enable greater time of service for these products.

Polyamide 66 (PA66) is a thermoplastic polymer widely used as matrix in CPN due to its excellent mechanical and thermal resistance, good barrier properties and recyclability (Okada and Usuki, 2006 and references therein). Photo-oxidation of PA66 occurs through a complex mechanism of chain breakage (Carroccio and Puglisi, 2004; Margolin et al., 1976; Thanki and Singh, 1998), which begins in the carbon atom adjacent to the amide group when a proton (H) is lost through the action of incident photons. This process generates a highly reactive free radical, which reacts by forming different intermediate groups (aldehyde, alkyl, carboxyl and hydroperoxide) to form degradation products that may or may not contain the intermediates, depending on the mechanism by which the reaction occurred. PA66 shows two mechanisms of photo-dissociation, termed Norrish I and Norrish II (Carroccio and Puglisi, 2004 and references therein). Both the intermediate and the final degradation products are highly reactive and non-accumulative, making it very difficult to predict the photo-dissociation

71 mechanism. PA66 is semi-crystalline; amorphous and crystalline zones coexist in its
72 structure. Due to its low permeability and high diffusion of O_2, the amorphous zone is
73 the zone most susceptible to photo-oxidation (Cerruti et al., 2005; Thanki and Singh,
74 1998), and the crystalline zone is affected superficially in shorter chains when most of
75 the amorphous zone has disappeared. Furthermore, photo-dissociation can cause some
76 amorphous chains to crystallize, making the material more fragile (Thanki et al., 2001).

77 Regarding photo-oxidative degradation of CPN, some studies performed on
78 polymers reinforced with montmorillonite (Mt) (Qin et al., 2004; Qin et al, 2005), it has
79 generally been observed that the clay nanoparticles accelerate the mechanism of CPN
80 degradation. Acceleration occurs because the remains of organic ammonium used in the
81 organophilization process of Mt can create initiation routes (active positions) for
82 degradation where the Fe^{3+} and Fe^{2+} from the Mt act as a catalyst (Bussière et al., 2013).
83 These effects are less severe when the clay used as reinforcing agent is a fibrous clay
84 (Bocchini et al., 2010). The fibrous habit of sepiolite (Sep) produces a network in the
85 polymer matrix that is less penetrable to oxygen, preventing the oxygen to react with the
86 polymer chains. In some cases, the Sep prevents the polymer from crystallizing with
87 photo-oxidation by causing immobility in the chains. In fact Sep has been used as a
88 stabilizing agent against photo-oxidation in other systems (Casal et al., 2001).

89 The aim of this work is to analyse how photo-oxidation affects the
90 crystallographic, mechanical, and optical properties of CPN Sep/PA66, taking into
91 account the degree of degradation caused through a standard accelerated degradation
92 method (UNE-EN-ISO 4892-2). For that purpose, a set of samples containing different
93 Sep percentage has been used: 0, 1, 3, 5, 7 and 9 wt.% (samples PA66-S-0, PA66-S-1,
94 PA66-S-3, PA66-S-5, PA66-S-7 and PA66-S-9, respectively). Prior studies have proved

the increasing of mechanical properties related to the individual phases and the good dispersion of the Sep in the polymer matrix (Fernández-Barranco et al., 2015).

2. Materials and Methods

The CPN studied in this work was manufactured with PA66 (Dinalon®, Grupo Repol, Spain) and organophilized sepiolite with a protonated quaternary ammonium salt (Tolsa S.A., Spain). The PA66 granulates and organosepiolite were previously dried in a vacuum oven during 24 h at 80ºC. Pellets were manufactured via melt intercalation using a double screw extruder (250 rpm, 250 °C), following the process described in a previous work (Yebra-Rodríguez et al., 2009).

The PA66 matrix was reinforced with different clay loading: 1, 3, 5, 7 and 9 wt.%, and the obtained samples were designated as PA66-S-1, PA66-S-3, PA66-S-5, PA66-S-7 and PA66-S-9, respectively. Neat PA66 was manufactured following the same procedure (sample PA66-S-0) to guarantee identical preparation conditions. The pellets of the samples were injected in an injection molding machine (BABYPLAST 6/10, CRONOPLAST) under the following conditions: tool pressure 25 MPa, cylinder temperature 285 C and tool temperature 50 °C. Two different injection molds were used: plate with 1 mm thickness (80 x 50 mm), and a specific mold according to the UNE-EN ISO 527-2 standard procedure. After injection, the CPN samples were exposed to radiation following the method described in the UNE-EN-ISO 4892-2 standard. A test chamber (SOLARBOX 1500e RH, COFOMEGRA) was used, with wide band of 300-400 nm and narrow-band of 340 nm. The cycle type was the number 2 from the method A, with constant irradiation (from a xenon arc) of 550 W/m^2 and 65 ± 3°C controlled by a Black Standard Thermometer (BST), without night. The relative humidity was controlled and monitored. An ultrasonic humidifier ensures reliable

functioning for long time. The total exposure time was 240 h; every 2 h the samples were immersed in deionizer water during 18 min. The resulting samples were designated as PA66-S-0_UV, PA66-S-1_UV, PA66-S-3_UV, PA66-S-5_UV, PA66-S-7_UV and PA66-S-9_UV.

Mechanical properties were determined using an Universal Testing Machine MTS Insight^{TM} with 5 kN load capacity, equipped with an extensometer and following the method described in UNE-EN ISO 527-1. Transparency was calculated with a non-contact SpectraScan PR-704 spectroradiometer (Photo Research, Chatsworth, USA) using the CIELAB method (Guinea et al., 2010). The degradation was quantified by the Carbonyl Index (CI) and Yellowness Index (YI). The infrared spectroscopic analyses (FT-IR) were used to obtain the Carbonyl Index. The samples were analysed in a FT-IR Bruker Tensor 27 spectrometer in the attenuated total reflection mode (ATR) between 400 and 4000 cm^{-1} at a resolution of 4 cm^{-1}. The CI was calculated from the spectra comparing the integrated area in the carbonyl region (1710 - 1760 cm^{-1}) with the CH_2 scissor bond region (1458 – 1468 cm^{-1}), which is unaffected by the degradation. The CI is defined as the ratio of the integrated carbonyl band and the reference band (Dong and Gijsman, 2010).

The ASTM provides a standard practice for calculating a yellowness index YI from instrumentally color coordinates (ASTM 313-96). This YI is as follows

$$YI = \frac{100(C_X X - C_Z Z)}{Y} \quad (1)$$

where X, Y and Z are the tristimulus values of the sample and C_X and C_Z are coefficients depending on the experimental conditions. With the illuminant/observer combination used in this experiment (D65/10°), values given by the ASTM for C_X and C_Z are 1.3013 and 1.1489, respectively. CIE tristimulus values X, Y and Z are the basic

values used to specify a color, and can be transformed to other colorimetric coordinates of other color systems. The International Commission on Illumination CIE (CIE, 1970, 1986, 2004) defined the tristimulus values as

$$V = \int_a^b W_V(\lambda)R(\lambda)d\lambda \qquad (2)$$

with $V = X, Y\ and\ Z$, where

$$W_X(\lambda) = \kappa S(\lambda)x(\lambda) \quad (3), W_Y(\lambda) = \kappa S(\lambda)y(\lambda) \quad (4), W_Z(\lambda) = \kappa S(\lambda)z(\lambda) \quad (5)$$

and where $S(\lambda)$ is the relative spectral power distribution of the illuminant (in our case, illuminant D65), $x(\lambda)$, $y(\lambda)$, and $z(\lambda)$ are the CIE standard observer color-matching functions (here, standard observer CIE1964 10°), $R(\lambda)$ is the spectral reflectance factor of the object color considered, (a-b) is the visible range of wavelengths (380-780 nm), and κ is a normalizing factor defined as follows

$$\kappa = 100/\int_a^b S(\lambda)y(\lambda)d\lambda \qquad (6)$$

These values X, Y and Z were obtained with a non-contact SpectraScan PR-704 spectroradiometer (Photo Research, Chatsworth, USA) with a 4% measurement accuracy and standard deviation of repeat measurements over a 15-minute period less than 0.1 % (Perez et al., 2000) following the method as described elsewhere (Yebra-Rodríguez et al., 2014).

Differential Scanning Calorimetry (DSC) was carried out in an equipment DSC 822e, Mettler Toledo. The samples were heated over the temperature range of 25-300 °C with a heating rate of 5 °C/min and under nitrogen flow (50mL/mm) for avoiding extra degradation. Crystallinity Index (W_c) was calculated from the ratio between the enthalpy of melting (ΔH_m), obtained for each sample from the area in the DSC curve

between onset and endset temperatures) and that of a fully crystalline PA66 sample (196 J/g, Lee and Phillips, 2007), according to the following formula, where w_{PA66} is the weight fraction of PA66:

$$W_c(\%) = \frac{\Delta H_m}{196\,J/g} \cdot \frac{100}{w_{PA66}} \qquad (7)$$

Diffraction patterns of the samples before and after photo-oxidative degradation were obtained with a X-ray Empyrean diffractometer with the PIXcel-3D detector (PANalytical, The Netherlands). The radiation was CuK_α (1.54178 Å) and the parameters: 40 kV and 35 mA. The range of the Bragg angle was between 2θ= 3 - 35°.

3. Results and discussion

The effects of the ultraviolet light and environmental oxygen on the samples after degradation are shown in Fig.1. In general, the values for yield stress (σ_m, Fig. 1A), Young's Modulus (E, Fig. 1B), and strain at break (ε_B, Fig. 1C) are lower in the degraded samples, indicating that the material generally loses mechanical properties due to degradation (Bussière et al., 2013; Dintcheva et al., 2010). The value of σ_m (Fig. 1A) is the least influenced by degradation, indicating that degraded CPN have similar tensile strength before and after degradation. In contrast, E decreases considerably during aging, a decrease greater than 1 GPa in all cases (Fig. 1B). The greatest loss of E occurs in the sample PA66-S-9_UV, which experiences a nearly 70% loss of stiffness. Reduction in elongation at break is common for all polymers after UV exposure, thus E is used for monitoring the aging of polymers (Torikai et al., 1990). The value of ε_B (Fig. 1C) is the value most influenced by UV exposure, and it decreases drastically after exposure. Even in CPN with little reinforcement (PA66-S-1_UV), loss of ε_B is greater than 81%. In the other CPN samples, the value of ε_B decreases more with higher

187 percentages of sepiolite, the most fragile sample being PA66-S-9_UV. This result
188 indicates that the nanocomposites embrittle with photo-oxidation without a drastic
189 decrease in tensile strength (Thanki et al., 2001). These results are associated with two
190 processes that compete as a consequence of UV exposure: chain scission and chain
191 crosslinking. Chain scission decreases the molecular weight and yield stress of
192 polymers, whereas chain crosslinking increases yield stress and embrittles polymers. As
193 a result of these processes the changes in yield stress are negligible.

194 The transparency values of the CPN samples before and after UV exposure (Fig.
195 2) show that the degraded samples display higher values than the undegraded samples,
196 being PA66-S-0_UV the most influenced sample after the photo-oxidative degradation
197 process. The tendency to increase in opacity as the percentage of sepiolite reinforcement
198 increases continues in the degraded samples, as the sepiolite renders specimen more
199 opaque. The changes in the mechanical and optical qualities of the CPN are due to their
200 structural modification, since exposure to light sources in the presence of O_2 affects the
201 polymer chains (Carroccio et al., 2003; Cerruti et al., 2005). The photons from the
202 ultraviolet radiation influence the polymer chains, breaking them and giving rise to new
203 C=O bonds and thus carbonyl groups, when the process of photo-dissociation occurs.

204 The indexes CI and YI (Figs. 3 and 4, respectively) were calculated to measure
205 the degree of degradation (through the extension of the C=O bonds) in the samples after
206 the photo-oxidation process. Fig. 3 compares the values of CI obtained for the samples
207 before and after degradation. The undegraded samples do not show a value of 0 for CI,
208 since the PA66 structure contains amide groups with C=O bonds detectable through FT-
209 IR. Furthermore, these bonds form with the breaking of the chains that occurs in the
210 extrusion and injection processes needed to obtain the CPN (Thanki, 1998). The value
211 of CI in the samples before degradation is lower than those in the degraded samples.

212 The highest value of CI corresponds to the sample PA66-S-0_UV. The aged
213 nanocomposites have a value close to that obtained in the undegraded samples and less
214 than that of the degraded sample without sepiolite (PA66-S-0_UV sample). Since the
215 degradation can occur by different mechanisms, Norrish I and Norrish II (Carroccio and
216 Puglisi, 2004), and may or may not be complete, the sepiolite prevents the
217 decomposition through a similar mechanism by which it occurs in neat PA66, a
218 mechanism that does not encourage the formation of C=O groups. In general, the
219 predominant decomposition mechanism of PA66 is Norrish I. This mechanism produces
220 a greater number of decomposition products (intermediate and/or final) with C=O bonds
221 in their formula. In contrast, the data obtained indicate that the presence of sepiolite
222 favours Norrish II, in which the products of decomposition have fewer C=O groups.
223 This mechanism is favoured by the structural organization of both phases in the
224 Clay/Polymer Nanocomposite and the good dispersion of the sepiolite in the polymer
225 matrix (Fernández-Barranco et al., 2016), which impedes the passage of O_2 and thus the
226 formation of C=O groups that would increase the CI. Thus, the sepiolite has an
227 inhibiting effect on the formation of C=O in the photo-oxidative degradation of the
228 polymer, as it also occurs in other oxidative degradation processes (Yebra-Rodriguez et
229 al., 2014). CPN samples with a value lower than 5 wt.% sepiolite show a CI value
230 closer to that of the undegraded samples (PA66-S-1_UV and PA66-S-3_UV), whereas
231 PA66-S-5_UV, PA66-S-7_UV, and PA66-S-9_UV (Fig. 4.5-3) show a tendency toward
232 increase in the CI. As the percentage of reinforcement increases (> 5 wt.%), the CI
233 increases, moving farther from the CI value in the undegraded samples. This increase in
234 degraded nanocomposite samples is always lower than that obtained for sample PA66-
235 S-0_UV.

The results of the YI obtained for the samples before and after UV exposure are shown in Fig.4. The YI values are similar in samples with similar content of sepiolite before and after photo-oxidative aging. The YI increases when the sepiolite content in the matrix increases but, in contrast to the other degradation processes, is not influenced by ultraviolet radiation (Yebra-Rodriguez et al., 2014). This occurs because exposure to ultraviolet light in the presence of oxygen does not cause degradation products such as pyrrole to form in the polymer and carbonaceous silicates in the case of the sepiolite, such that the yellowness of the nanocomposites does not change (Levchik et al., 1999).

Table 1 displays the calculated crystallinity index and melting temperature (T_m) of the studied samples. The crystallinity index (W_c) depends on the quantity of sepiolite and has an oscillating tendency which is also observed in the degraded CPN. W_c varies in a similar way when the Clay/Polymer Nanocomposite is degraded, such that photo-oxidation does not produce a relevant change in W_c. Some studies show that photo-oxidative degradation of polymers begins in the amorphous zone, as O_2 penetrates more easily there (Cerruti et al., 2005; Thanki et al., 2001). In this case, the effect is reflected in the values of melting temperature before and after degradation. The values of T_m increase slightly or remains the same in all degraded samples, and less in the sample PA66-S-9_UV, in relation to the undegraded samples. This phenomenon contrasts with what occurs in other PA66 systems, where degradation does affect the crystalline zone (Cerruti et al., 2005; Cerruti and Carfagna, 2010). This increase involves a reduction in the amorphous zones, which are generally melted more easily than the crystalline zones. Further, these results show signs of recrystallization in the amorphous zone, which contributes to the embrittlement of the CPN, hence the loss of mechanical properties (E and ε_B), which indicate loss of ductibility (Figs. 1B and 1C).

The loss of amorphous zones in the PA66 is also reflected in the diffraction patterns of the CPN (Fig. 5). The zone of the diffraction pattern between 5-12 °2θ displays a shoulder that spans the whole range, typically corresponding to the amorphous region in the polymer structure. This shoulder disappears in the degraded samples, confirming the partial collapse of the amorphous zone already observed after DSC analyses (T_m, Table 1). The Bragg angle of the diffraction peaks of the PA66 α structure (20.3 °2θ and 23.2 °2θ, corresponding to the planes (100) and (010)/(110), respectively) (Bunn and Garner, 1947) are not affected by degradation, since the spacing between adjacent planes remains unchanged by either the action of the sepiolite rods (which are placed perpendicular to the PA66 lamellae through hydrogen bonds without modifying the PA66 chains) or the degradation. However, the loss of amorphous region provokes an increase in the intensity of PA66 diffraction peaks in the degraded samples with low sepiolite content (PA66-S-0_UV, PA66-S-1_UV, and PA66-S-3_UV). Photo-oxidation promotes the recrystallization of the PA66, according to the results obtained in the transparency test (Fig. 2). The characteristic peaks of the CPN structure (Fernández-Barranco et al., 2018), which appear at 8.70 °2θ, 17.55 °2θ, 26.03 °2θ and 32.86 °2θ in the nanocomposites containing 5 wt.% of sepiolite and above, remain after degradation of the samples and sharpen in the diffractions patterns of the nanocomposite containing the highest percentage of sepiolite (PA66-S-9_UV sample, Fig. 5D). The degradation of the amorphous region in these samples promotes the ordering of the CPN structure, in which the sepiolite fibers place between adjacent PA66 adjacent lamellae and trigger higher order degree in the CPN suprastructure. However, the crystallinity index (Table 1) shows that, despite increasing the ordering of the structure, the crystallite size of the polymer is necessarily smaller. Moreover, according to the tensile tests (linked to the crystallinity of the sample), the more

crystalline a material, the greater its resistance, which fits the results shown in Fig. 1A. The loss of amorphous zones (more ductile) and recrystallization of PA66 causes the embrittlement of the CPN, as shown in Fig. 1C.

4. Conclusions

The behaviour of nanocomposites Sep/PA66 was evaluated after photo-oxidative exposure. Mechanical properties and transparency of the Clay/Polymer Nanocomposites are clearly affected. A high reduction of ductility, resulting in an embrittlement, has been observed. After UV exposure, samples are more translucent and therefore more crystalline when the percentage of Sep increases in the CPN. Carbonyl indices of nanocomposite samples are lower than those of neat PA66, which indicates that sepiolite nanofibers prevent the formation of carboxyl bonds. DSC and XRD analyses demonstrate that the ageing of nanocomposites starts in the amorphous zone of PA66, thus the Clay/Polymer nanocomposites present higher crystallinity degree after UV exposure (i.e. the amount of crystals increases), although the crystals are not more prefect. The more crystalline and the greater resistance of the new material is in concordance with the mechanical analyses. Loss of amorphous (more ductile) zones and crystallization of some chains cause the CPN to embrittle considerably. The crosslinking structure formed between Sep and PA66 impedes the diffusion of oxygen in the hybrid, which acts as a catalyser in the UV degradation. That is, sepiolite has an inhibitory effect in the photo-oxidative degradation of Clay/Polymer nanocomposites.

Acknowledgments

This research was supported by Centro de Estudios Avanzados en Ciencias de la Tierra (University of Jaén, Spain), Andalusian Research Groups RNM-325, TEP-138 (CICE,

JA, Spain). The authors thank CICT (University of Jaén, Spain), CIC (University of Granada, Spain), and the technicians for data collection.

References

Bocchini, S., Fukushima, K., Di Blasio, A., Fina, A., Frache, A., Geoblado, F., 2010. Polylactic acid and polylactic acid-based nanocomposite photooxidation. Biomacromolecules 11, 2919-2926.

Bunn, C.W., Garner, E.V., 1947. The crystal structures of two polyamides ("nylons"). Proc. R. Soc. of A 189, 39-68.

Bussière, P.O., Peyrouz, J., Chadeyron, G., 2013. Influence of functional nanoparticles on the photostability of polymer materials: recent progress and further applications. Polym. Degrad. Stab., 98(12), 2411-2418.

Butnaru, E., Cheaburu, C.N., Yilmaz, O., Pricope, G.M., Vasile, C., 2016. Poly(vinyl alcohol)/chitosan/montmorillonite nanocomposites for food packaging applications: Influence of montmorillonite content. High Perform. Polym., 28, 1124-1138.

Carroccio, S., Puglisi, C. 2004. MALDI investigation of the photooxidation of nylon66. Macromolecules, 37, 6037-6049.

Carroccio, S., Puglisi, C., Montaudo, G., 2003. New vistas in the photo-oxidation of nylon 6. Macromolecules, 36, 7499-7507.

Casal, B., Merino, J., Serratosa, J.M., Ruiz-Hitzky, E., 2001. Sepiolite based materials for the photo- and thermal stabilization of pesticides. Appl. Clay Sci. 18, 245-254.

CIE Publication 15:2004. Colorimetry, 3rd edition. Vienna: CIE Central Bureau; 2004.

Cerruti, P., Carfagna, C., 2010. Thermal-oxidative degradation of polyamide 6,6 containing metal salts. Polym. Degrab. Stab., 95, 2405-2412.

Cerruti, P., Lavorgna, M., Carfagna, C., Nicolais, L., 2005. Comparision of photo-oxidative degradation of polyamide 6,6 films stabilized with HALS and $CuCl_2$ + KI mixtures. Polymer, 46, 4571-4583.

Dintcheva, N.Tz., Filippone, G., La Mantia, F.P., Acierno, D., 2010. Photo-oxidation behaviour of polyethylene/polyamide 6 blends filled with organomodified clay: Improvement of the photo-resistance through morphology modification. Polym Degrad. Stab. 2010, 95, 527-535.

Dong, W., Gijsman, P., 2010. Influence of temperature on the thermo-oxidative degradation of polyamide 6 films. Polym. Degrad. Stab. 95, 1054–1062.

Fernández-Barranco, C., Koziol, A.E., Drewniak, M., Yebra-Rodriguez, A., 2018. Structural characterization of sepiolite/polyamide6,6 nanocomposites by means of static and dynamic thermal methods. App. Clay Sci., 153, 154-160.

Fernández-Barranco, C., Koziol, A.E., Skrzypiec, K., Rawski, M., Drewniak, M., Yebra-Rodriguez A., 2016. Study of spatial distribution of sepiolite in polyamide 66/sepiolite nanocomposites. App. Clay Sci., 127-128, 129-133.

Fernández-Barranco, C., Yebra-Rodríguez, A., La Rubia-García, M.D., Navas-Martos, F.J., Alvarez-Lloret, P., 2015. Mechanical and crystallographic properties of injection-molded polyamide 66/sepiolite nanocomposites with different clay loading. Polym. Composite, 36, 2326-2333.

353 Guinea, R., Pérez, M.M., Herrera, L.J., Rivas, M.J., Yebra, A., Paravina, R.D., 2010.
354 Color difference thesholds in dental ceramics. J Dent., 38(2), e57-e64.

355 Lee, S.S., Phillips, P.J., 2007. Melt crystallized polyamide 6.6 and its copolymers, Part
356 I. Melting point – Lamellar thickness relations in the homopolymer. Eur. Polym.
357 J., 43, 1933-1951.

358 Kotal M, Bhowmick AK., 2015. Polymer nanocomposites from modified clays: recent
359 advances and challenges. Prog Polymer Sci, 51, 127-187.

360 Levchik, S.V., Weil, E.D., Lewin, M., 1999. Thermal decomposition of aliphatic
361 nylons. Polym. Int. 48, 532–557.

362 Margolin, A.L., Kabanova, I.A., Postnikov, L.M., Shlyapintokh, V.Ya, 1976. On the
363 pho-oxidation of aliphatic polyamides. Vysokomol soyed, A18(5), 1094-1099.

364 Mukhopadhyay, R., Bhaduri, D., Sarkar, B., Rusmin, R., Hou, D., Khanam, R., Sarkar,
365 S., Kumar Biswas, J., Vithanage, M., Bhatnagar, A., Ok, Y.S., 2020. Clay–
366 polymer nanocomposites: Progress and challenges for use in sustainable water
367 treatment. J. Hazard. Mater. 383, 121-125.

368 Okada, A., Usuki, A., 2006. Twenty years of polymer-clay nanocomposites. Macromol.
369 Mater. Eng. 291:1449-1476.

370 Olewnik-Kruszkowska, E., 2015. Effect of UV irradiation on thermal properties of
371 nanocomposites based on polylactide. J. Therm. Anal. Calorim., 119, 219–228.

372 Pandey, J.K., Reddy, R., Kumar, A.P., Singh, R.P., 2005. An overview on the
373 degradability of polymer nanocomposites. Polym. Degrad. Stab., 88, 234–250.

374 Pérez, M.M., Melgosa, M., El Moraghi, A., Hita, E., 2000. Usefulness of cathode ray
375 tube color displays in chromaticity–discrimination experiments. Appl. Optics 22,
376 4021–4030.

377 Pfaendner, R., 2010. Nanocomposites: industrial opportunity or challenge? Polym.
378 Degrad. Stab., 95, 369-373.

379 Qin, H., Zhang, Z., Feng, M., Gong, F., Zhang, S., Yang, M., 2004. The influence of
380 interlayer cations on the photo-oxidative degradation of
381 polyethylene/montmorillonite composites. J. Polym. Sci. Part B Polym. Phys. 42,
382 3006-30012.

383 Qin, H., Zhang, S., Liu, H., Xie, S., Yang, M., Shen, D., 2005. Photo-oxidative
384 degradation of polypropylene/montmorillonite nanocomposites. Polymer, 46,
385 3149-3156.

386 Remili, C., Kaci, M., Hachbi, S., Bruzaud, S., Grohens, Y., 2009. Photo-oxidation of
387 polystyrene/clay nanocomposites under accelerated UV exposure: effect on the
388 structure and molecular weight. J. Appl. Polym. Sci., 112, 2868-2875.

389 Sharma, B., Jain, P., Purwar, R., 2019. Preparation and characterization of poly(vinyl
390 alcohol)/modified clay electrospun nanocomposite nanofibrous mats for microbial
391 protection. J. Text I., 110, 1624-1634.

392 Thanki, P.N., Ramesh, C., Singh, R.P., 2001. Photo-irradiation induced morphological
393 changes in nylon 66, Polymer 42:535-538.

394 Thanki, P.N., Singh, R,P., 1998. Photo-oxidative degradation of nylon 66 under
395 accelerated weathering. Polymer, 39(25), 6363-6367.

396 Torikai, A., Shirakawa, H., Nagaya, S., Fueki, K. Photodegradation of polyethylene:
397 factors affecting photostability., 1999. J. Appl. Polym. Sci. 40:1637-1646.

398 Yebra-Rodríguez, A., Alvarez-Lloret, P., Cardell, C., Rodríguez-Navarro, A.B., 2009.
399 Crystalline properties of injection molded polyamide-6 and polyamide-
400 6/montmorillonite nanocomposites. App. Clay Sci., 43, 91-97.

401 Yebra-Rodríguez, A., Fernández-Barranco, C., La Rubia-García, M.D., Yebra, A,
402 Rodríguez-Navarro, A. B, Jiménez-Millán, J., 2014. Thermooxidative degradation
403 of injection molded sepiolite/polyamide66 nanocomposites. Min. Mag. 78(5),
404 1227-1239.

405 Valino AD, Dizon JRC, Espera AH, Chen Q, Advincula RC., 2019. Advances in 3d
406 Printing of Thermoplastic Polymer Composites and Nanocomposites. Prog. Polym.
407 Sci., 98, 1-19.

408 Zaidi, L., Kaci, M., Bruzaud, S., Bourmaud, A., Grohens, Y., 2010. Effect of natural
409 weather on the structure and properties of polylactide/cloisite 30B
410 nanocomposites. Polym. Degrad. Stab, 95, 1751–1758.

411

412 **FIGURE CAPTIONS**

413 **Fig. 1.** Mechanical properties of the CPN samples before and after photo-oxidative
414 degradation. A) Yield Stress, B) Young's Modulus C) Strain at Break**.**

415 **Fig. 02.** Transparency data of the studied samples before and after photo-oxidative
416 degradation. Less than ± 0.1 error.

417 **Fig. 3.** Carbonyl Index with standard deviation before and after photo-oxidative
418 degradation.

419 **Fig. 4.** Yellowness Index of the CPN samples before and after photo-oxidativ**e**
420 degradation. Less than ± 0.01 error.

421 **Fig.5.** Diffraction patterns of Sep and neat PA66 (A) and the samples with 1 (B), 5 (C)
422 and 9 (D) wt.% of sepiolite loading, before and after photo-oxidative degradation.

423

Graphical Abstract

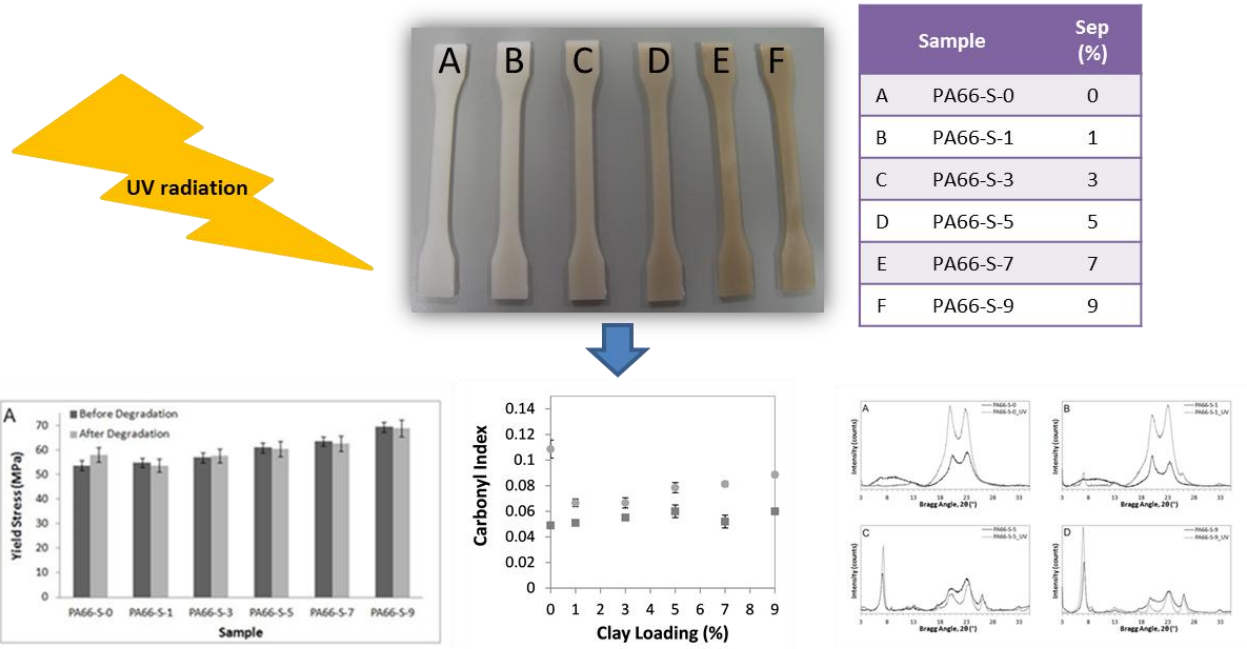

- The influence of the sepiolite on the behavior of the nanocomposites after UV exposure has been studied.
- Sepiolite has an inhibitor effect on the formation of C=O.
- The crystallographic arrangement of PA66 and sepiolite hinders the oxygen diffusion.
- The breaking of chains is lower in nanocomposites due of the sepiolite.

Table 1. Thermal data and crystallinity index from DSC of the samples before and after photo-oxidative degradation. Less than ± 0.1 error.

Sample	W_c (%)	T_{onset} (°C)	T_m (°C)	T_{endset} (°C)
PA66-S-0	37.2	257.2	265.2	269.0
PA66-S-1	34.0	256.2	264.8	269.1
PA66-S-3	34.3	254.9	264.9	270.7
PA66-S-5	35.0	256.2	264.1	269.3
PA66-S-7	33.7	255.1	264.3	270.5
PA66-S-9	30.9	252.5	264.0	268.7
PA66-S-0_UV	35.5	256.6	266.4	271.3
PA66-S-1_UV	36.0	259.7	266.7	269.5
PA66-S-3_UV	32.6	254.3	264.9	269.2
PA66-S-5_UV	33.3	253.3	264.6	268.4
PA66-S-7_UV	32.6	257.4	265.0	269.0
PA66-S-9_UV	32.3	250.3	263.6	268.1

Figure 1

Click here to download Figure: Fig1.xlsx

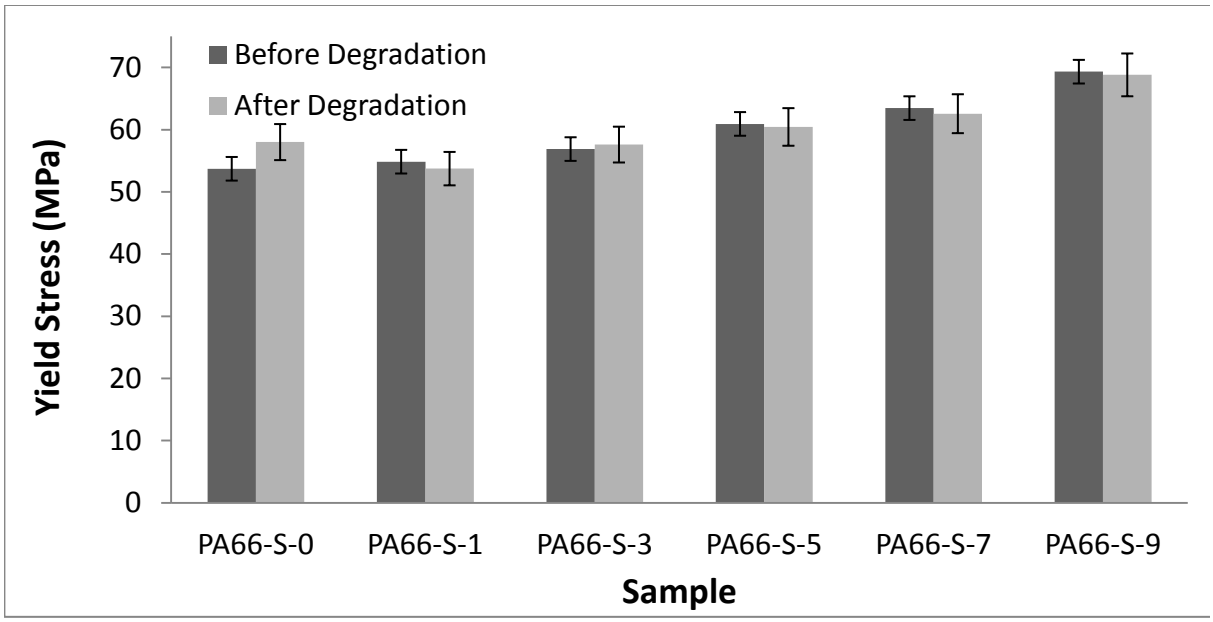

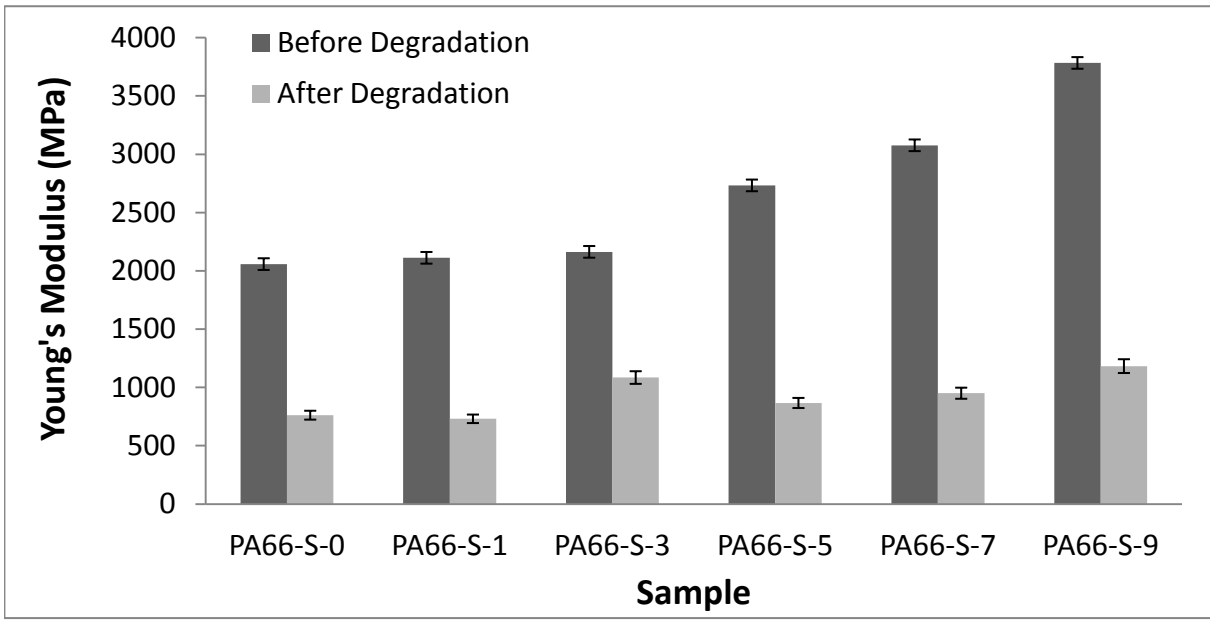

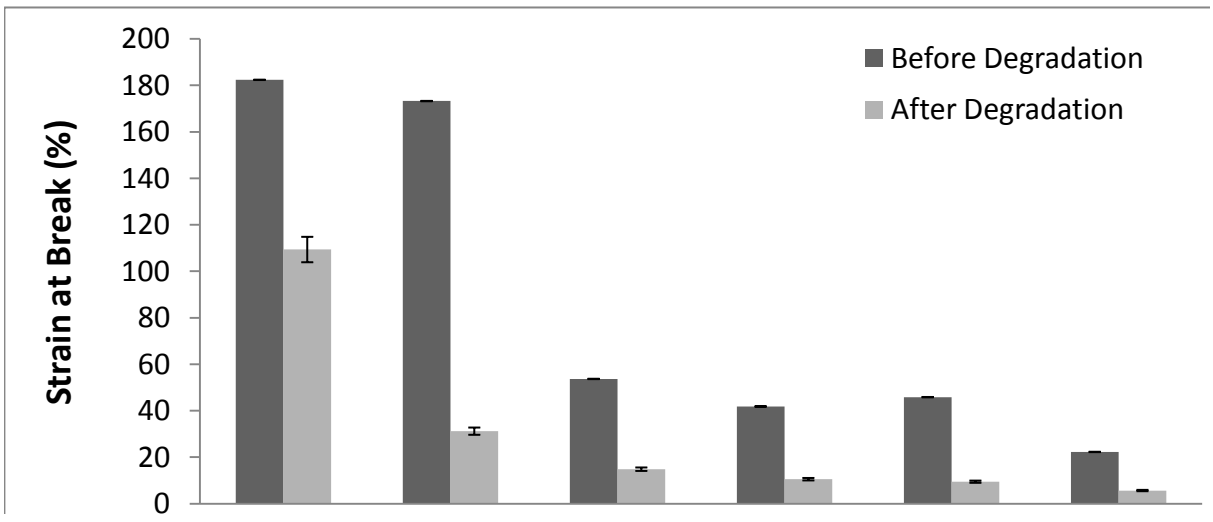

Figure 2
Click here to download high resolution image

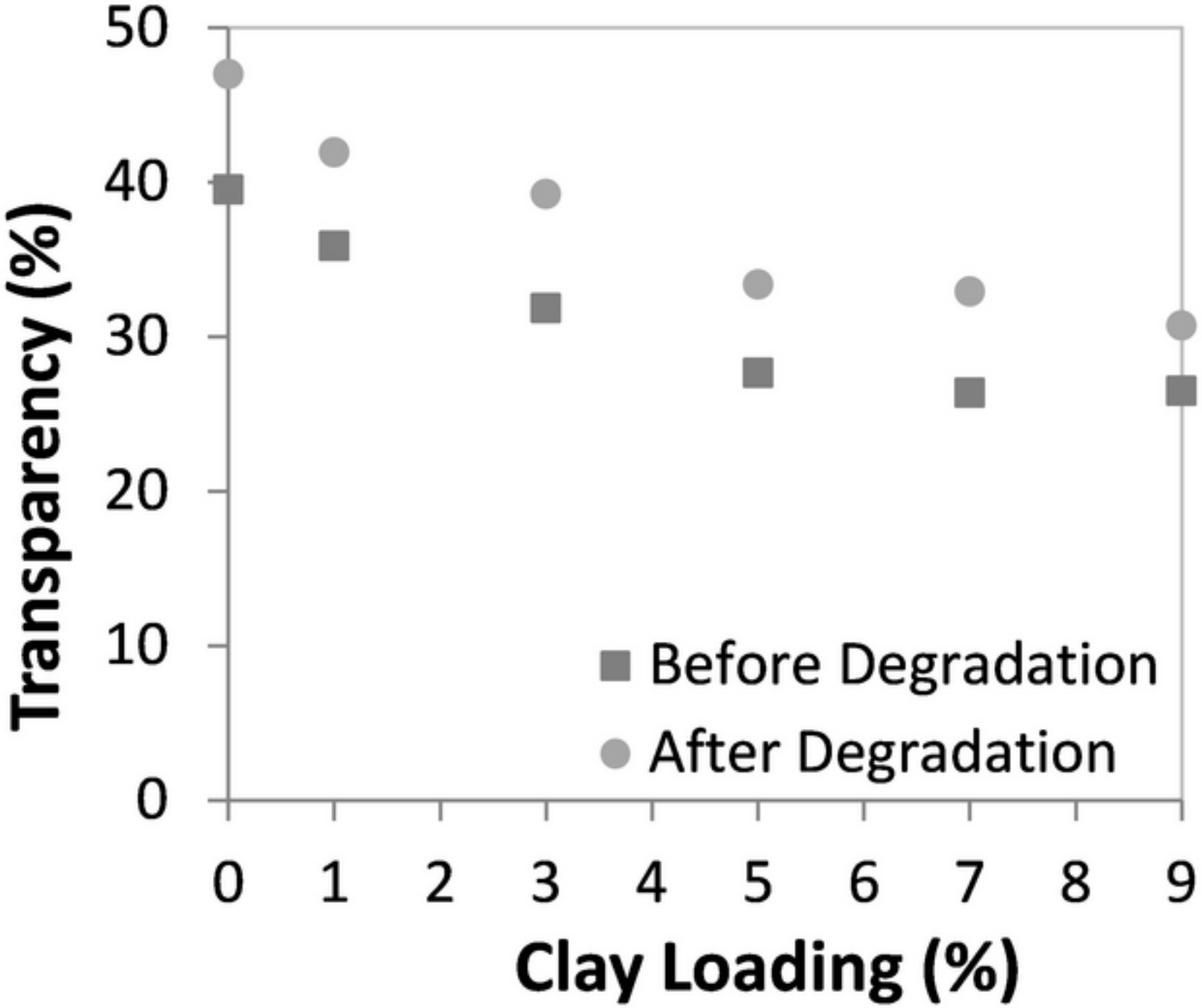

Figure 3
Click here to download high resolution image

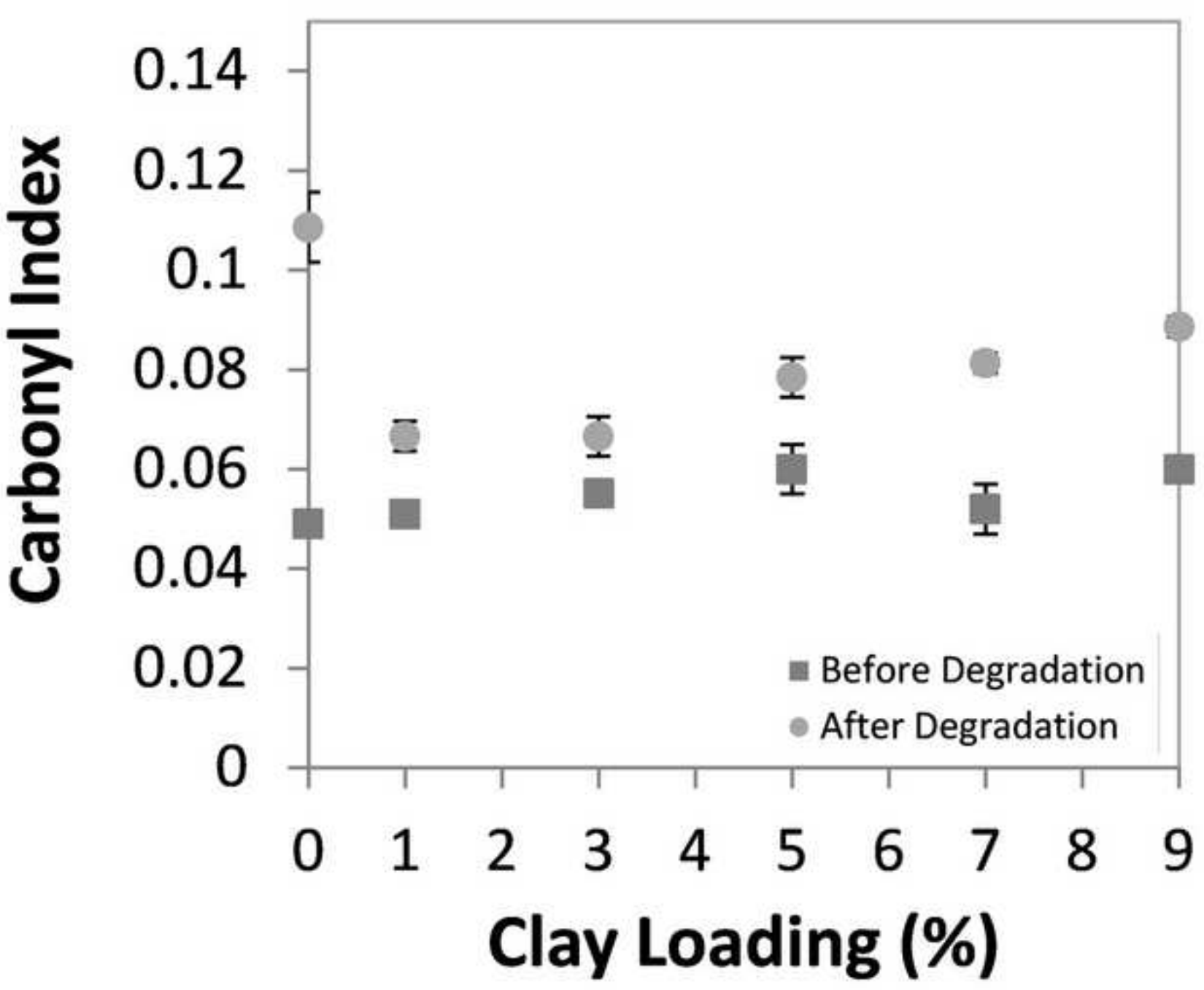

Figure 4

Click here to download high resolution image

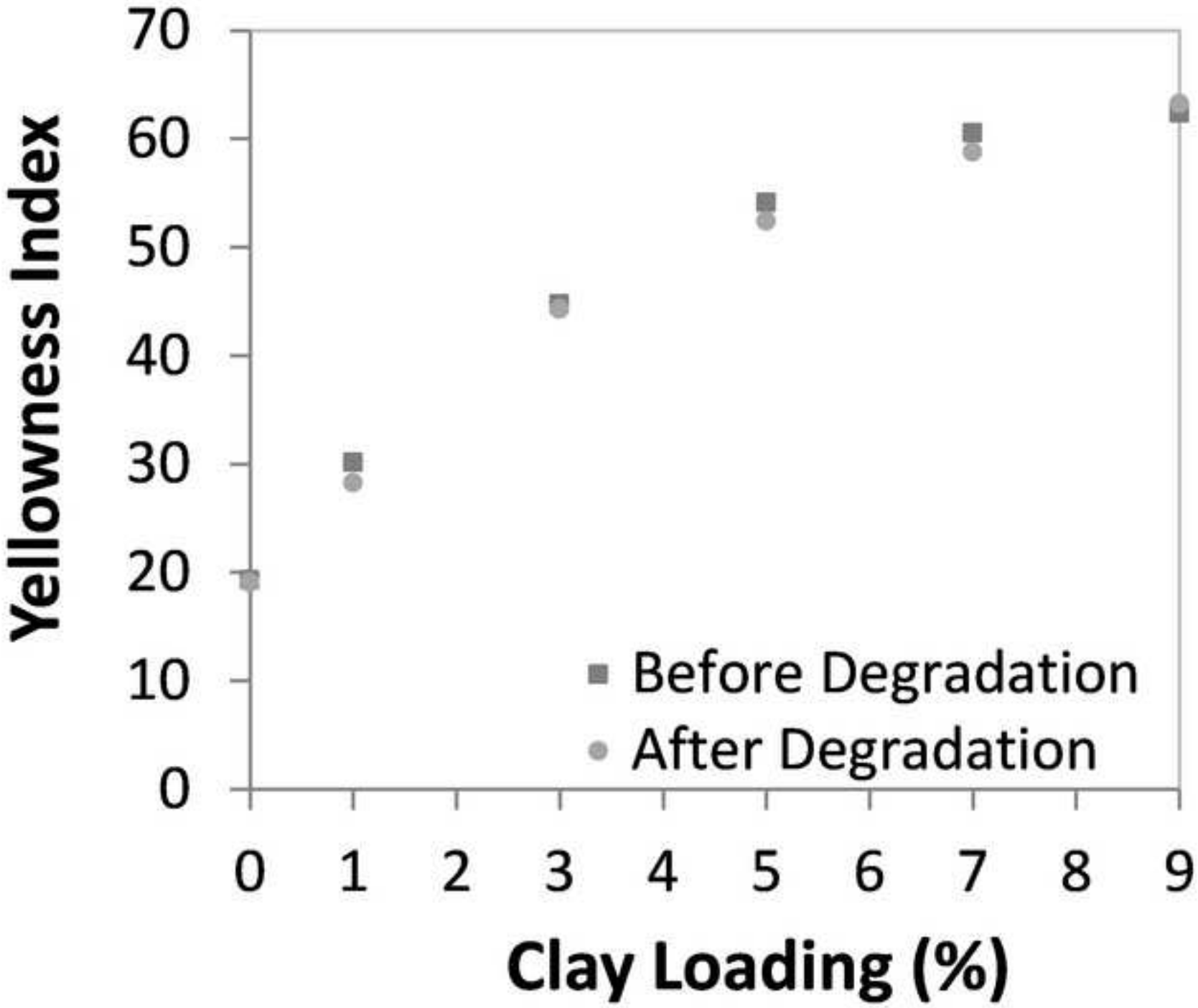

Figure 5

Click here to download Figure: Fig5.xlsx

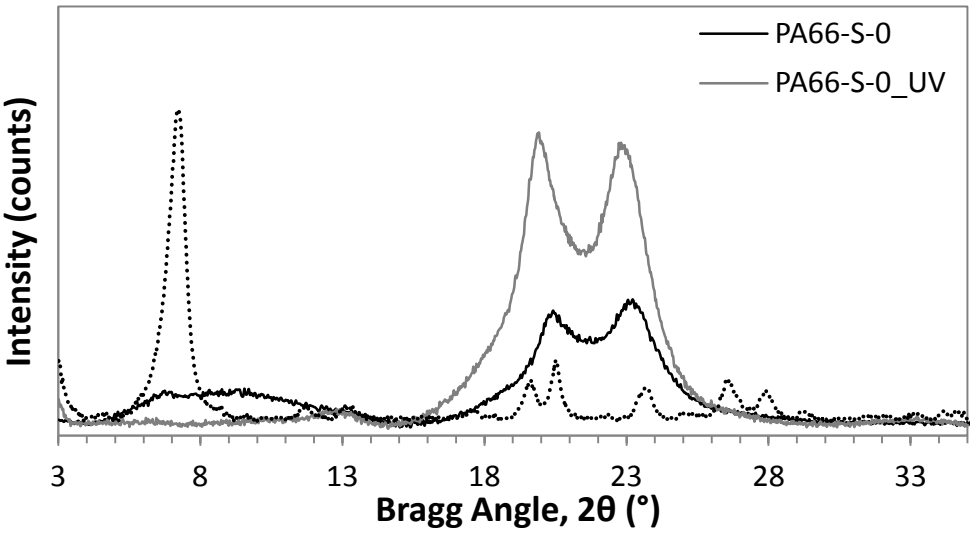

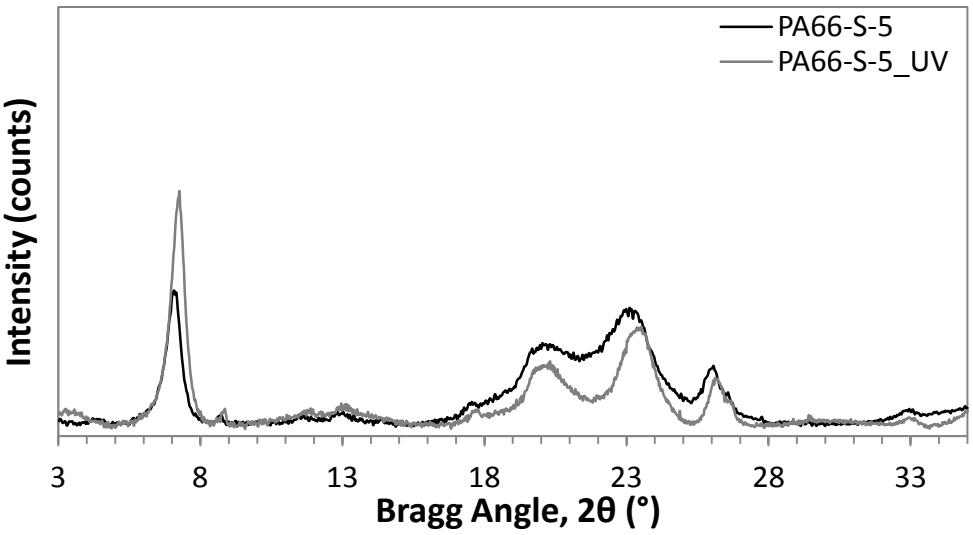

***Declaration of Interest Statement**

Declaration of interests

☒ The authors declare that they have no known competing financial interests or personal relationships that could have appeared to influence the work reported in this paper.

☐The authors declare the following financial interests/personal relationships which may be considered as potential competing interests:

M. Dolores La Rubia

***Credit Author Statement**

C. Fernández-Barranco: Investigation, writing the original draft preparation. F. J. Navas-Martos: Validation, formal analysis. A. Yebra: Optical investigation. A. Yebra-Rodríguez and M. Dolores La Rubia: Conceptulization, methodology, Writing-Reviewing and Editing. J. Jiménez-Millán and A. E. Koziol Supervision: